ADVANCED ENERGY MATERIALS
www.advenergymat.de

Enhanced Electrocatalytic CO_2 Reduction to C_{2+} Products by Adjusting the Local Reaction Environment with Polymer Binders

Thi Ha My Pham, Jie Zhang, Mo Li, Tzu-Hsien Shen, Youngdon Ko, Vasiliki Tileli, Wen Luo, and Andreas Züttel*

The activity and selectivity of the electrochemical CO_2 reduction reaction (CO_2RR) are often hindered by the limited access of CO_2 to the catalyst surface and overtaken by the competing hydrogen evolution reaction. Herein, it is revealed that polymers used as catalyst binders can effectively modulate the accessibility of CO_2 relative to H_2O at the vicinity of the catalyst and thus the performance of CO_2RR. Three polymers with different hydrophilicities (i.e., polyacrylic acid (PAA), Nafion, and fluorinated ethylene propylene (FEP)) are selected as binders for Cu catalysts. At a thickness of only ≈1.2 nm, these binders strongly affect the activity and selectivity toward multi-carbon (C_{2+}) products. The FEP coated catalyst exhibits a C_{2+} partial current density of over 600 mA cm^{-2} with ≈77% faradaic efficiency at −0.76 V versus RHE. This high performance is attributed to the hydrophobic (aerophilic) properties of FEP, which reduces the local concentration of H_2O and enhances that of the reactant (i.e., CO_2) and the reaction intermediates (i.e., CO). These findings suggest that tuning the hydrophobicity of electrocatalysts with polymer binders can be a promising way to regulate the performance of electrochemical reactions involving gas–solid–liquid interfaces.

1. Introduction

Over the past century, an excessive amount of CO_2 has been released into the atmosphere due to the consumption of fossil fuels, giving rise to climate change and other environmental problems.[1,2] A zero-emission energy economy is no longer sufficient; the discharged carbon in the atmosphere must be sequestrated. Recently, electrochemical CO_2 reduction reactions (CO_2RR) enabled by renewable energy have been suggested as a promising strategy to solve these problems, sequestrating discharged CO_2 into chemical feedstocks, and downscaling the use of fossil fuels in the chemical production industry. In addition, CO_2RR is an efficient way to store electricity generated from intermittent renewable energies in the form of liquid fuels for transport and other applications.[3–5]

Copper-based materials are the most investigated class of catalysts for CO_2RR due to their unique ability to reduce CO_2 molecules to carbonaceous compounds containing more than two carbon atoms (C_{2+} products). However, the high overpotential required and the low product selectivity over the pristine Cu surface have motivated researchers to develop more efficient strategies to overcome these challenges. Most previous publications have focused on engineering the properties of Cu-based catalysts, such as optimizing the size and shape of Cu nanomaterials,[6–10] introducing grain boundaries,[11] and creating alloys with other metals[12–15] to increase the number of active sites and/or to improve the intrinsic catalytic activities of Cu toward the desired products. Despite the tremendous progress that has been made, CO_2RR is still not viable at an industrial scale.

T. H. M. Pham, J. Zhang, M. Li, Y. Ko, W. Luo, A. Züttel
Laboratory of Materials for Renewable Energy (LMER)
Institute of Chemical Sciences and Engineering (ISIC)
Basic Science Faculty (SB)
Ecole Polytechnique Fédérale de Lausanne (EPFL) Valis/Wallis
Energypolis, Rue de l'Industrie 17, Sion CH-1951, Switzerland

The ORCID identification number(s) for the author(s) of this article can be found under https://doi.org/10.1002/aenm.202103663.

DOI: 10.1002/aenm.202103663

T. H. M. Pham, J. Zhang, M. Li, Y. Ko, W. Luo, A. Züttel
EMPA Materials & Technology
Dübendorf CH-8600, Switzerland

T.-H. Shen, V. Tileli
Institute of Materials (IMX)
Ecole Polytechnique Fédérale de Lausanne (EPFL)
Lausanne CH-1015, Switzerland

W. Luo
School of Environmental and Chemical Engineering
Shanghai University
99 Shangda Road, Shanghai 200444, China
E-mail: wenluo@shu.edu.cn

The performance of a catalytic reaction, however, is not only affected by the catalyst. It is also influenced by reaction pressure, temperature, ratio of reactants, etc. In the case of CO_2RR, the reaction is mostly carried out at room temperature and at ambient pressure conditions; hence, tuning the ratio of reactants becomes a practical and attractive strategy to improve the performance of CO_2RR. Since H_2O and CO_2 are the reactants for aqueous CO_2RR, and the hydrogen evolution reaction (HER) from H_2O is the competitive reaction that limits the CO_2RR selectivity, it is reasonable to optimize the ratio of H_2O and CO_2 to suppress H_2 evolution and enhance the electrolysis of CO_2. In a conventional H-cell reactor, the electrode is immersed in the electrolyte, and CO_2 molecules dissolve in the electrolyte and diffuse to the surface of the electrode. Thus, the ratio of CO_2 to H_2O is always limited by the low solubility and slow diffusion of CO_2, particularly at high current densities.[16] Using a flow reactor can overcome this limitation, as the supply of CO_2 and H_2O is separated by the gas diffusion electrode (GDE).[17,18] However, GDEs tend to lose their hydrophobicity during CO_2RR, leading to the flooding of the electrodes and, consequently, a decrease in CO_2 mass transport.[19,20] To maintain a higher CO_2 to H_2O ratio, researchers have tried to coat Cu surfaces with a relatively thick layer of polymer or ionomer.[21–23] This strategy, however, may decrease the conductivity of the electrode and block the active sites of the catalyst.[21]

On the other hand, polymers are often used to bind catalyst powders onto the supporting material (e.g., carbon paper), and Nafion is an almost universal binder selection for catalysts used in CO_2RR due to its good proton conductivity. However, little attention has been paid to whether Nafion is the most suitable binder for Cu catalysts used in CO_2RR, and how the hydrophobicity of polymer binders affects the catalytic performance. Here, we used three types of polymers, such as polyacrylic acid (PAA) and fluorinated ethylene propylene (FEP), as binders for Cu catalysts, and revealed that their distinct hydrophobic properties can change the transport of H_2O and CO_2 to the electrode surface, thus greatly affecting the activity and selectivity of CO_2RR. We observed an enhanced selectivity toward carbonaceous products, particularly in C_{2+} products, induced by the hydrophobicity of the FEP binder. We also observed an increased H_2 selectivity induced by a hydrophilic binder (i.e., PAA). Specifically, with FEP as a binder, we achieved ≈50% Faradaic efficiency (FE) for C_{2+} at −1.1 V versus RHE in a conventional H-cell and ≈77% C_{2+} FE at −0.76 V versus RHE in a flow cell. In addition, we confirmed the important role of polymer binders in tuning the local environment through ex situ and in situ characterizations. Since polymer binders are widely used in electrochemical reactions, including CO_2, CO, and N_2 reduction reactions, we believe that this work is of great importance to researchers from these fields and we anticipate that screening of polymer binders will be an important step in the future studies.

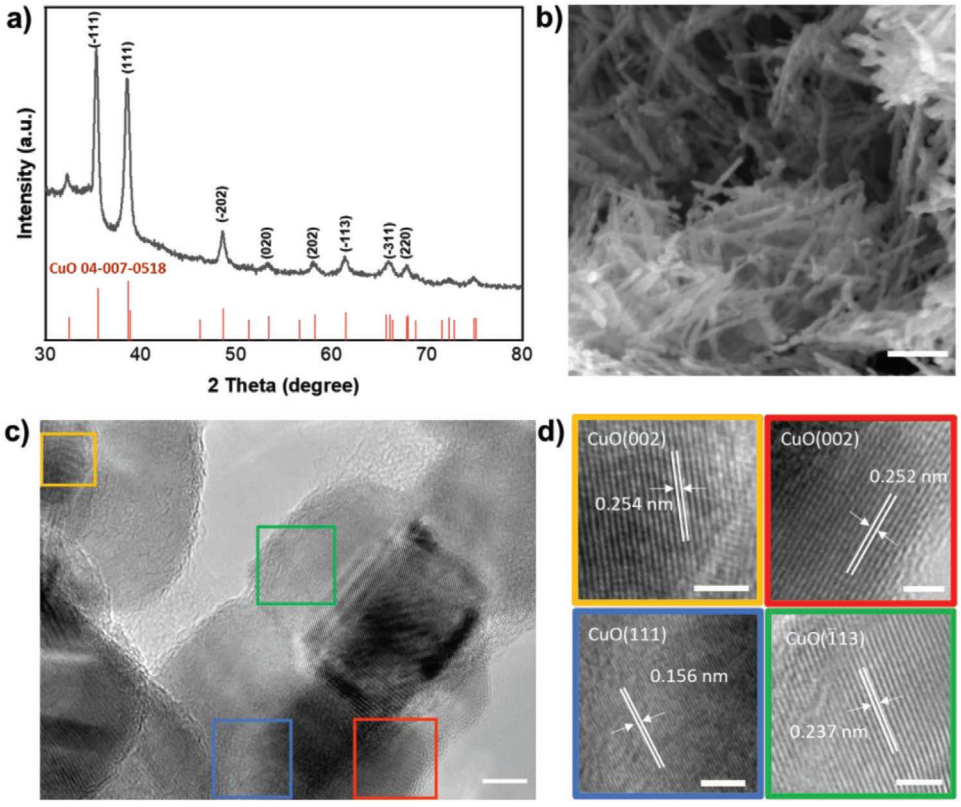

Figure 1. Physical characterizations of the as-synthesized powder catalysts. a) XRD pattern of the as-synthesized catalyst including the diffraction lines of CuO from the Powder Diffraction File database. b) Needle-like structure of the as-synthesized CuO with an aspect ratio of 6 to 10. (SEM image, scale bar: 200 nm). c) Selected grains of as-synthesized CuO (HR-TEM image, scale bar: 10 nm). d) Magnified image of the areas outlined in Figure 1c. (HR-TEM images, Scale bar: 2 nm).

2. Results and Discussions

2.1. Characterization of the Copper Electrode

CuO was synthesized from $Cu(NO_3)_2$ and NaOH through a simple precipitation method and used as a representative Cu catalyst in this work. The X-ray diffraction (XRD) spectrum confirmed that the obtained material was pure polycrystalline CuO (**Figure 1**a). The morphology of CuO was studied using scanning electron microscopy (SEM), and a highly porous structure was revealed (Figure S1, Supporting Information). Close-up analysis of the CuO material reveals that the porous structure was built out of CuO needles, which have a length of several hundred nanometers and a width of 10–20 nm (Figure 1b). The high-resolution transmission electron microscopy (HR-TEM) images acquired at the edge of a CuO needle indicates that the needle was composed of small grains with a well-defined crystal structure (Figure S2a, Supporting Information) and rich in grain boundaries (Figure S2b, Supporting Information). Figure 1c shows HR-TEM images of particles with grains corresponding to various crystalline planes. Figure 1d is composed of four representative grains with well-defined d-spacings between the crystalline planes, which can be attributed to the exposure of (002), (111), and ($\bar{1}$13) facets (Figure S2c, Supporting Information), verifying the polycrystalline nature of the as-synthesized CuO catalyst.

For preparing the working electrode, we chose three types of polymers that have different hydrophobicities as binders: (1) PAA, which only has hydrophilic functional groups; (2) Nafion, which has both hydrophobic and hydrophilic functionalities; and (3) FEP, which only has hydrophobic functional groups (chemical formulae shown in Figure S3, Supporting Information). The CuO powder and the polymer binder (0.2 mg mg^{-1} catalyst) were simply mixed in iso-propanol, sonicated for dispersing, and drop-casted to prepare the electrode. The distribution of the polymer binder on the powder catalyst was first studied using SEM energy-dispersive X-ray spectroscopy (SEM-EDX). **Figure 2**a shows an SEM image and its corresponding EDX map of the Cu-PAA sample, where the map of carbon present in PAA strongly overlaps with that of Cu, indicating that PAA is uniformly distributed on the CuO needles. Similar results were also obtained for Cu-Nafion and Cu-FEP, as indicated by the overlap of the elemental map of F and those of Cu and O (Figure S4, Supporting Information). In addition, energy-filtered TEM (EF-TEM) was used to investigate the coverage of the polymer layer on the powder catalyst. Figure 2b shows the bright-field TEM image of CuO particles coated with the PAA polymer. The corresponding EF-TEM carbon elemental map in Figure 2c using core-loss carbon K edge electron energy-loss spectra (EELS) corroborates the fact that the carbonaceous polymer layer was homogeneously coated on the surface of the CuO particles. The TEM images in Figure S5 (Supporting Information) also show that the coating layer had a thickness of around 1.2 nm for all three samples. Thus, these results demonstrate that a simple method involving physical mixing and ultrasonication is sufficient to coat the surface of the CuO powder with a thin layer of polymer binder.

The surface properties of polymer-coated CuO samples were studied using X-ray photoelectron spectroscopy (XPS). For this measurement, the three dispersions were drop-casted on clean Au foils to ensure good conductivity and to avoid the influence of other elements. On all three samples, the presence of polymer binder on the CuO surface was confirmed, with C—O,

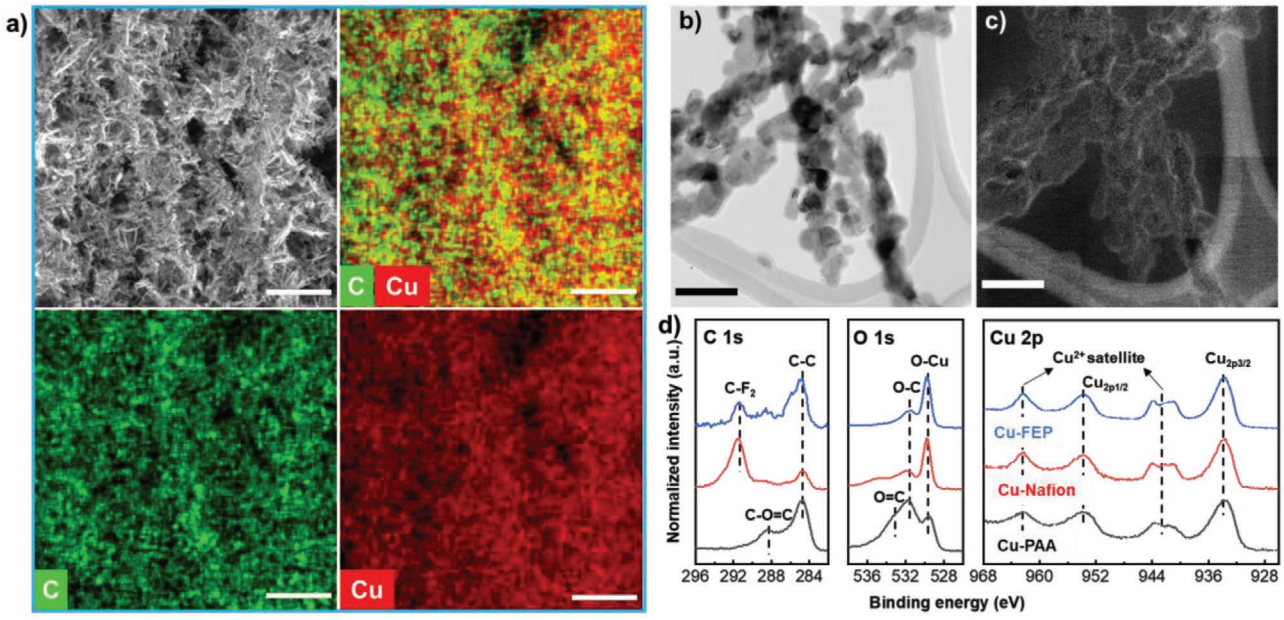

Figure 2. Morphology and chemical composition of the Cu-polymer catalysts. a) Cu-PAA drop-casted on a Ni foil (SEM image and the corresponding elemental map of Cu and C, scale bar: 1 µm). A clean Ni foil was used as a substrate to avoid the influence of other elements. b) Morphology of CuO (bright-field TEM image, Scale bar: 50 nm) and c) the corresponding carbon distribution of the Cu-PAA catalyst (EF-TEM carbon elemental map, Scale bar: 50 nm). d) Surface chemistry of the three Cu-polymer catalysts (XPS spectra for C 1s, O 1s, and Cu 2p, respectively); a clean Au foil was used for good conductivity and to avoid the influence of other elements.

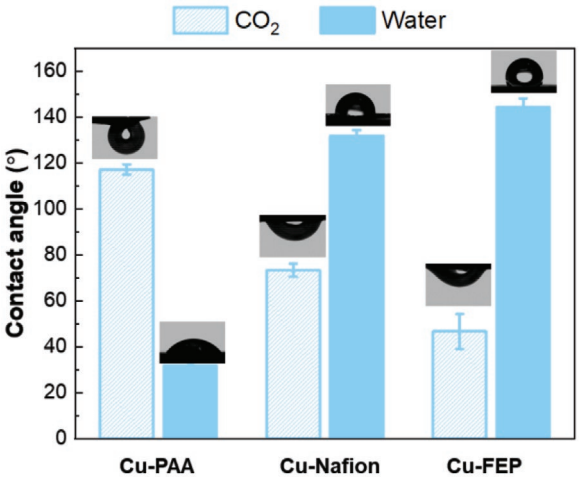

Figure 3. Characterization of the hydrophilicity and CO_2-philicity of the Cu-polymer catalysts. The water- and CO_2-contact angles of each catalyst were determined by the tangent method. Water contact angle: filled, CO_2 captive contact angle: striped.

C=O, and C−F peaks clearly observable in the C 1s and O 1s region in the XPS spectra (Figure 2d). All samples show typical Cu 2p spectra of CuO, indicated by the presence of Cu $2p_{3/2}$ peak at ≈933.6 eV as well as high-intensity satellite peaks. In addition, no peaks related to Cu−F or Cu−S bonding were detected, demonstrating that coating of polymer binder did not change the chemical properties of CuO.

To evaluate the effect of different polymer binders on the hydrophobicity of Cu-based electrodes, we performed the water contact angle (WCA) and the captive bubble contact angle (CBCA) measurements. **Figure 3** shows that the WCA for Cu-PAA, Cu-Nafion, and Cu-FEP were 32°, 132°, and 144°, respectively, corresponding to an increasing trend in hydrophobicity. On the other hand, the measured CBCA followed an opposite trend compared to the WCA (Figure 3): the contact angle for the CO_2 bubble increased from Cu-FEP (47°) to Cu-Nafion (73°) and Cu-PAA (117°). These results indicate that a thin layer of polymer binder can successfully change the hydrophobicity of the electrode. With PAA as a binder, the electrode surface is highly hydrophilic, hindering the access of CO_2 toward the surface of the catalyst during CO_2RR. In contrast, for Cu-FEP electrodes, the hydrophobic nature of FEP favors the accumulation of CO_2 gas, thus can increase its local concentration near the catalyst. Overall, from the comprehensive characterizations above, we can conclude that Cu-based catalysts coated with a thin layer of three different polymer binders were successfully synthesized. The hydrophobicity of the electrode was effectively tuned by the hydrophilic or hydrophobic properties of the polymer binder, which is expected to change the ratio of reactants (H_2O and CO_2) near the surface of the electrode.

2.2. CO_2RR Performance

To evaluate the effect of the polymer binder on the catalytic performance of the as-synthesized Cu-based catalysts, we first performed CO_2RR tests in a conventional H-cell in CO_2-saturated 0.1 M $KHCO_3$ at potentials ranging from –0.6 to –1.2 V versus RHE (product distributions are shown in Figure S7, Supporting Information, with bare Cu sample as reference). The FEs of H_2 on CuO-derived catalysts with three different binders were plotted against the applied potential (**Figure 4**a). The H_2 selectivity was significantly suppressed in the entire potential range by the hydrophobic polymer, compared to a hydrophilic polymer such as PAA. Consequently, the total FEs for CO_2RR (FEs for CO, formate, CH_4, C_2H_4, *n*-propanol, ethanol, and acetate) increased with the polymer's hydrophobicity and aerophilicity (Figure S8a, Supporting Information). We further analyzed the product distribution of CO_2RR and plotted the FEs for C_{2+} products (C_2H_4, *n*-propanol, ethanol, and acetate) and C_1 products (CO, HCOOH, and CH_4) in Figure 4b and Figure S8b (Supporting Information), respectively. As shown in Figure 4b, C_{2+} products can be detected at potentials from –0.7 V versus RHE for all three samples, and the FEs increased with the hydrophobicity of the surface: Cu-FEP > Cu-Nafion > Cu-PAA. The highest FE of C_{2+} products (≈52%) was reached on the CuO-FEP electrode at –1.1 V versus RHE at a partial current density of 37.4 mA cm^{-2}. In addition, the enhancement of the CO_2RR selectivity by the hydrophobic polymer is more significant for C_{2+} than that for C_1 products, especially at high overpotentials. As shown in Figure S8c (Supporting Information), the maximum ratio of C_{2+} FE to C_1 FE for the Cu-FEP electrode was 5.5, while the ratio for the Cu-PAA sample was only 2. These results suggest that the polymer binder plays a significant role in enhancing the selectivity of CO_2RR, especially for C_{2+} products, while suppressing the selectivity of H_2.

In addition to product selectivity, the current density of CO_2RR was also affected by the polymer binder. As shown in Figure 4c, at a high overpotential range (–1.0 to –1.2 V versus RHE), the overall current density of Cu-FEP was higher than that of Cu-Nafion and Cu-PAA. The high current density of Cu-FEP was mainly attributable to the increased partial current density for CO_2RR rather than HER (Figure S9 a,b, Supporting Information). This indicates that even with a thin hydrophobic polymer layer on the catalyst surface, the H_2O supply in the H-cell was still sufficient for HER, and the enhanced CO_2 local concentration was the key to improved CO_2RR activity and C_{2+} selectivity. Further, we evaluated the effect of binder content on catalytic performance. As shown in Figure S10 (Supporting Information), a low level of FEP (0.05 mg mg^{-1} catalyst) could not effectively promote the reduction of CO_2 to C_{2+} products, while an excessive amount of FEP (0.8 mg mg^{-1} catalyst) led to thick coatings that blocked the active surface of the catalyst, again demonstrating the important role of polymer binders in electrocatalysis.

After the performance tests, the morphology and the hydrophobicity of the used catalysts were studied. The highly porous network and the needle-like structure of CuO remained intact for all three samples, as demonstrated in the SEM images (Figure S11, Supporting Information). Also, the polymer layers coated on the CuO needles are preserved (Figure S11 c,f,i, Supporting Information). In consequence, the WCAs of the three used samples are very similar to that of the fresh sample, indicating that the initial CuO reduction and the following CO_2 electrolysis processes did not change the hydrophobicity of the catalysts (Figure S12, Supporting Information). During the long-term test, the current density and FE for C_2H_4 remained stable for Cu-FEP (Figure 4e) and Cu-Nafion (Figure S13a, Supporting Information), while a

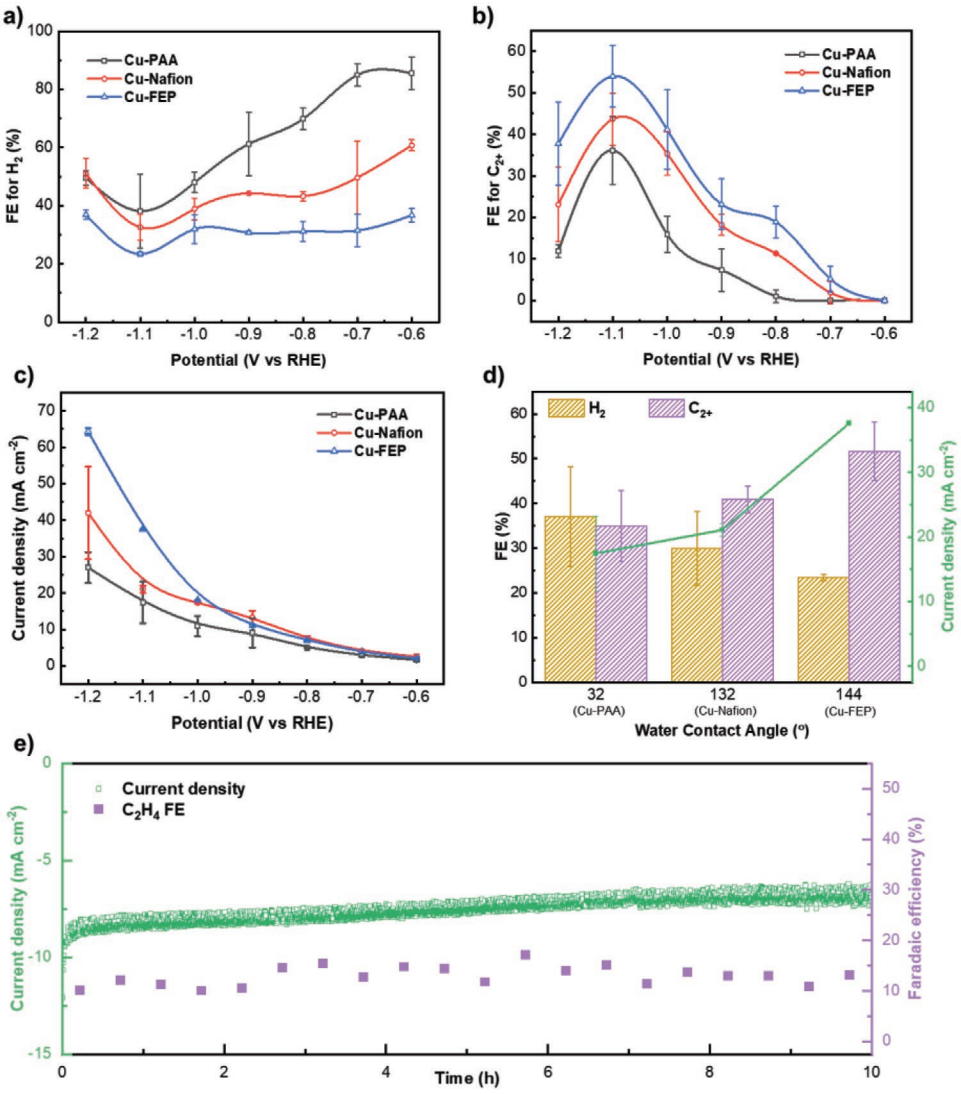

Figure 4. a) Faradaic efficiency of H_2, b) faradaic efficiency C_{2+} products, and c) Total current density for Cu-PAA, Cu-Nafion, and Cu-FEP. d) Total current density and FEs for H_2 and C_{2+} products as a function of the hydrophilicity, acquired in H-cell at –1.1 V versus RHE. e) Current density and C_2H_4 selectivity for Cu-FEP over 10 h of CO_2RR, acquired in H-cell at –0.8 V versus RHE.

decrease of FE for C_2H_4 and fluctuations in current density were observed due to the wetting of the Cu-PAA electrode (Figure S13b, Supporting Information). Overall, a good correlation between the CO_2RR performance and the surface hydrophobicity can be established (Figure 4d), and this correlation can be further extended to other polymer binders (Figure S14, Supporting Information).

As we have shown above, although the hydrophobic layer can dramatically improve the performance of CO_2RR in the H-cell, both the current density and C_{2+} selectivity are still limited by the low CO_2 concentration ($\approx 34 \times 10^{-3}$ M L^{-1}). To overcome the limitations of CO_2-solubility, we performed CO_2 electrolysis in a flow cell where the CO_2 supply and H_2O supply were decoupled by a gas diffusion electrode (GDE). The experiments were performed at constant current densities of 50, 100, 200, 300, 400, and 800 mA cm^{-2} using 1.0 M KOH as an electrolyte, and product distributions are shown in Figure S15 (Supporting Information). Similar to the H-cell, the use of hydrophobic binder suppressed significantly the HER over the whole range of overpotential (Figure S16, Supporting Information). **Figure 5**a shows the FEs of C_{2+} products for the Cu-FEP, Cu-Nafion, and Cu-PAA samples. The C_{2+} selectivity of Cu-FEP and Cu-Nafion increased continuously with a decrease in the applied potential, unlike in the H-cell where volcano-shaped curves were observed. This trend can be explained by the absence of the limitation of CO_2 mass transport in the flow reactor even at much higher current densities. However, the volcano-shaped C_{2+} FE curve was still observed for Cu-PAA, where the C_{2+} FE reached a maximum of 49% between –0.5 and –0.6 V versus RHE, and then dropped down to only 13% at –0.88 V versus RHE. This was mainly due to the low hydrophobicity of the Cu-PAA electrode that led to severe flooding, and hence limited CO_2 transport at higher overpotential ranges, as salt crystals were clearly observed on the CO_2-gas side of the GDE after only

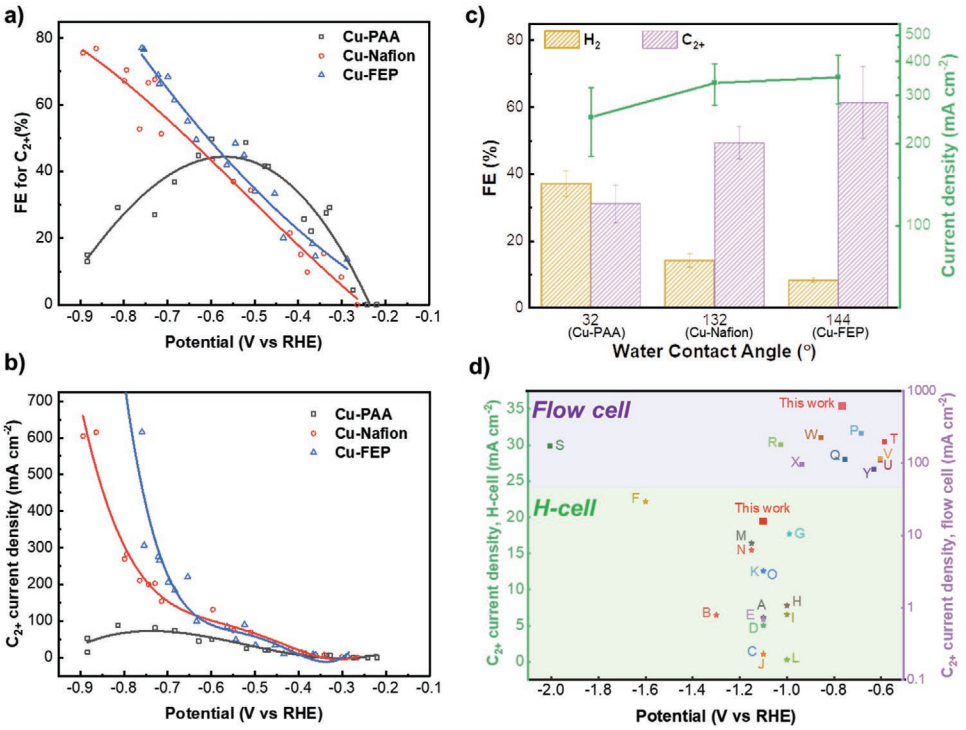

Figure 5. a) Faradaic efficiency for C_{2+} products, b) Partial current density for C_{2+} products, and c) Total current density and FEs for H_2 and C_{2+} products as a function of the hydrophilicity, acquired in flow cell at –0.71 V versus RHE, with aqueous 1.0 M KOH as electrolyte. d) C_{2+} production rate (represented as partial current density) as a function of the potential. The Cu-FEP catalyst compared with other reported CO_2RR catalysts obtained in H-cells (star) and flow cells (square). Details of each catalyst and the reported reactions conditions are provided in Tables S2 and S3 (Supporting Information).

a few minutes of reaction (Figure S17, Supporting Information). Notably, at –0.76 V versus RHE, Cu-FEP showed the highest C_{2+} FE of ≈77% toward C_{2+} products and a partial current density of more than 600 mA cm^{-2} (Figure 5b). Cu-Nafion also reached similar FE and current density but at a more negative potential (–0.86 V versus RHE). In the case of the hydrophilic Cu-PAA sample, the best partial current density for C_{2+} was 87.6 mA cm^{-2} at –0.81 V versus RHE, approximately eight times lower than that of the Cu-FEP and Cu-Nafion samples. Thus, similar to that of the H-cell, the binder's hydrophobicity correlates well to the activity and selectivity of the Cu catalysts in the flow reactor, as summarized in Figure 5c and Figure S14b (Supporting Information). By performing additional control experiments using the spray-coating method to prepare GDE,[24] we further confirm that this hydrophobicity–performance correlation is also applicable for electrodes prepared by other methods (Figure S18, Supporting Information).

Previous studies have shown that electrodes are much less stable in flow cells than that in H-cells due to the flooding issue. However, we find that the stability of the GDE can be significantly improved with a hydrophobic binder. For the Cu-FEP electrode, no flooding was observed after 16 h of stability test at 200 mA cm^{-2} in 1.0 M KOH, and the FE for C_2H_4 even increased slightly with the increase of reaction time (Figure S19a, Supporting Information). In comparison, after 10 h test, the Cu-Nafion electrode became less stable at 200 mA cm^{-2} and the Cu-PAA electrode was completely flooded at only 50 mA cm^{-2}. Notably, the morphology of Cu nanowires changed during the reaction, which is similar to previous observations that Cu catalysts undergo reconstruction.[25] The reconstruction is more obvious for the Cu-PAA sample, as the needle-like structure of Cu changed to a particle structure after 15 min of CO_2 electrolysis at 50 mA cm^{-2} (Figure S20, Supporting Information). After a longer reaction time, the morphology reconstruction takes place for all three samples (Figure S21, Supporting Information). However, EDX maps showed that polymer binders remained on the electrode and their signals overlapped with that of Cu (Figure S21b,c, Supporting Information), explaining the high stability of the Cu-FEP sample.

We also compared the performance of the Cu-FEP sample with the reported state-of-the-art Cu-based catalysts in H-cells[8,21,33–36,22,26–32] and flow cells[18,24,37–41] (Figure 5d), in terms of the partial current density and the applied potential. It is clear that in both the H-cell and flow cell reactors, our Cu-FEP sample is among the best Cu-based catalysts documented in the literature, showcasing high C_{2+} selectivity and current density at relatively low overpotentials. These results demonstrate that optimizing the hydrophobicity of the electrode with a polymer binder is a simple yet highly effective way of enhancing the CO_2RR performance of Cu-based catalysts.

2.3. Investigation into the Mechanism of C_{2+} Enhancement

To gain insight into the enhanced C_{2+} selectivity observed on the hydrophobic electrode, we monitored the reduction process of the CuO and intermediates of CO_2RR using operando surface-enhanced Raman spectroscopy (SERS). As shown in **Figure 6**,

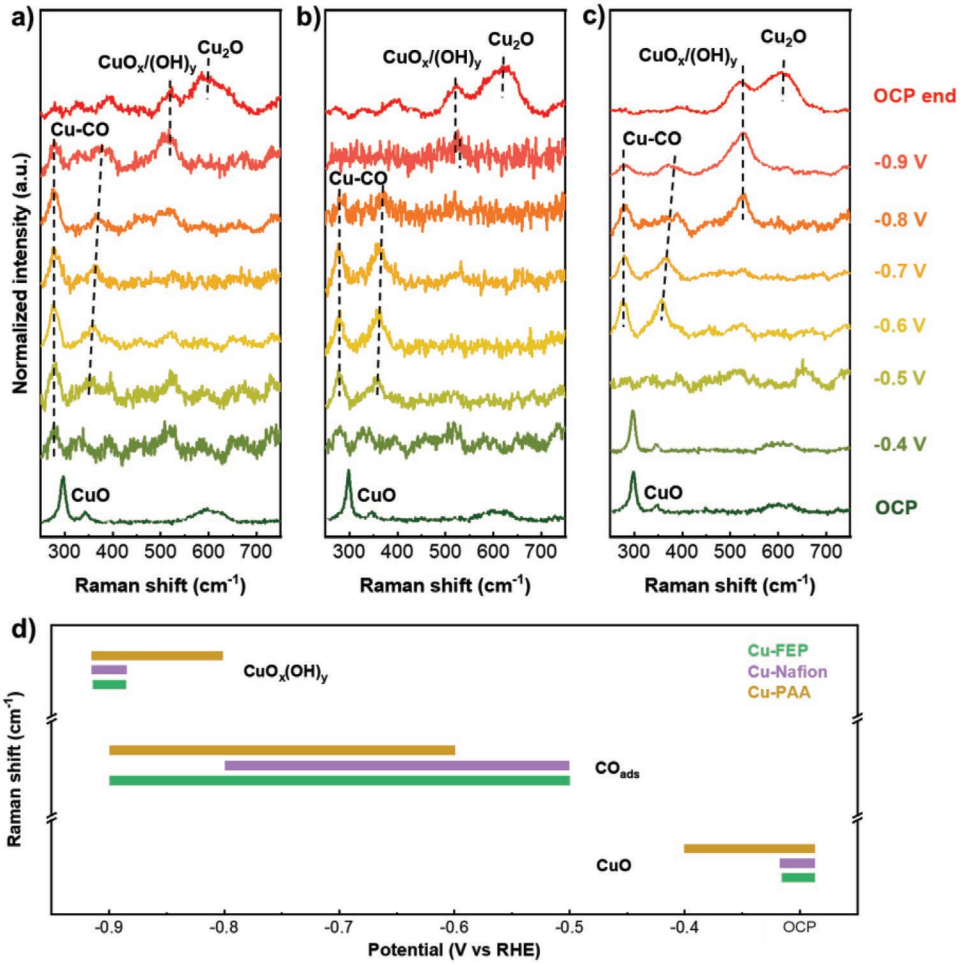

Figure 6. Operando Raman spectra of a) Cu-FEP, b) Cu-Nafion, and c) Cu-PAA. From bottom to top: initial OCP, –0.4 to –0.9 V versus RHE, final OCP. d) Adsorbed species ($CuO_x(OH)_y$, CO_{ads}, CuO) present at the surface of the three working electrodes (Cu-FEP, Cu-Nafion, Cu-PAA) during the CO_2RR, identified by operando Raman. The detection of each surface species at their characteristic Raman shifts was presented with respect to the applied potential.

for all three samples, two distinct peaks at 298 and 340 cm^{-1} and one broad peak ranging between 570 and 650 cm^{-1} were observed at open circuit potential (OCP), which are originated from cupric oxide (CuO).[42,43] When –0.4 V versus RHE was applied, all of the above peaks disappeared from the Cu-Nafion and Cu-FEP spectra, indicating that the Cu samples were completely reduced to Cu. In the case of Cu-PAA, these peaks disappeared at –0.5 V versus RHE, suggesting that the reduction of Cu to metallic Cu is more sluggish compared to the other two cases. This may be attributed to the slightly denser and thicker layer of PAA coating around the powder catalyst due to its higher solubility (Figure S5, Supporting Information).

After the complete reduction of Cu, several Raman peaks related to the adsorbed CO appeared. Two peaks at 280 and 367 cm^{-1} were attributed to the rotation of CO_{ads} on Cu and the stretching of metal-molecular bond, respectively[14,30,44,45] (Figure 6); a broad band ranging between 2000 and 2093 cm^{-1} was attributed to the internal stretching of CO molecule (Figure S22, Supporting Information). This broad peak was composed of two adjacent peaks: the first peak at 2000 cm^{-1} corresponded to the CO_{atop} configuration, and the second peak at 2093 cm^{-1} arose from the CO_{bridge} configuration.[45] These peaks became more clearly defined at moderate overpotentials (–0.6 and –0.7 V versus RHE), indicative of a greater degree of CO coverage at this potential range. We also observed a blue shift in the metal-molecular stretching as the potential became more negative, which had been previously attributed to the electrochemical Stark effect.[46,47] Starting from –0.9 V versus RHE for Cu-FEP and Cu-Nafion, and from –0.8 V versus RHE for Cu-PAA, a new peak at 520 cm^{-1} appeared. This was reported to be from adsorbed OH_{ads} on the Cu surface, originating from the high local pH near the catalyst surface due to the consumption of protons by CO_2RR and HER.[48] After removing the potential, no intermediate peaks were detected, but a new broad peak indicative of cuprous oxide appeared at 610–625 cm^{-1}.[45] Thus, we can conclude that metallic copper is the active site for CO_2RR, and is responsible for adsorbing the key reaction intermediate, CO, for C_{2+} products.

The results above can be correlated with the electrochemical performance of the catalysts. Figure 6d summarized the presence of adsorbed species on the catalyst surface at various applied potentials. The CO adsorption peaks were observed in a wider potential range (–0.5 to –0.9 V versus RHE) for Cu-FEP compared to that for Cu-Nafion (–0.5 to –0.8 V versus RHE) and Cu-PAA (–0.6 to –0.9 V versus RHE). The enhanced CO

chemisorption can be attributed to the high production rate of CO (Figure S23, Supporting Information) induced by the high local concentration of CO_2 on the surface, as well as to the accumulation of CO on the catalyst surface thanks to the hydrophobicity of the polymer binder. As CO is the key intermediate for C_{2+} products, the presence of these CO chemisorption peaks at low overpotentials, as well as over a wide potential range, explains why Cu-FEP produced more C_{2+} products over the entire potential range compared to Cu-Nafion and Cu-PAA.

While the contact angle measurements shed light on how the ratio between CO_2 and H_2O was responsible for the enhanced CO_2RR selectivity, the operando Raman measurements suggest that the ratio between CO and H_2O plays a key role in tuning the C_{2+} selectivity. To further verify these results, we carried out control experiments on a catalyst with better CO selectivity (Figure S24, Supporting Information): the Au-nanoparticle-decorated CuO catalyst (Figure S24a,b, Supporting Information). Catalysts with the three different polymer binders were denoted as Au@Cu-PAA, Au@Cu-Nafion, and Au@Cu-FEP. We also evaluated these samples in an H-cell using 0.1 M $KHCO_3$ as the electrolyte. As expected, the Au@Cu-FEP catalyst, which contains the most hydrophobic polymer binder, exhibited the highest CO_2RR selectivity due to the highest local CO_2 concentration (Figure S24c, Supporting Information). However, its C_{2+} selectivity was lower than that of Au@Cu-Nafion (Figure S24d, Supporting Information). Since Au is highly selective for CO but not active for HER, the Au@Cu surface was expected to require more protons to further reduce the adsorbed CO toward C_{2+} products compared to a pure Cu catalyst. Consequently, when the binder is partially hydrophilic, as is the case of Au@Cu-Nafion, the reduction of CO is more efficient, resulting in greater C_{2+} selectivity. These results, together with those observed from Cu-polymer catalysts, allow us to conclude that the hydrophobicity of polymer binders can effectively regulate the activity and selectivity of CO_2RR by tuning the local concentrations of reactants (i.e., CO_2 and H_2O) and intermediates (i.e., CO).

Based on the results described above, the mechanism of CO_2RR over Cu-polymer binder catalysts is illustrated in **Figure 7**. In an H-cell, Cu particles are coated with a layer of binder, the electrolyte is CO_2-saturated, and both protons and CO_2 have to access the catalyst surface through the electrolyte. In the case of Cu-PAA, due to the hydrophilic nature of the binder, the surface of the catalyst is covered by the electrolyte such that the CO_2 concentration is much lower than H_2O (33 mmol L^{-1} for CO_2 compared to 55 mol L^{-1} for H_2O; Figure 7a). For Cu-FEP, due to the high hydrophobicity of FEP, there exist local channels around the catalyst where only CO_2-vapor can access the electrode, thus increasing the local concentration of CO_2 and enhancing CO_2RR (Figure 7b). In a flow cell, the catalyst is drop-casted on the microporous layer (MPL) side of the GDE, and CO_2 is introduced from the other side. The reaction takes place at the triple-phase boundary where the catalyst is in contact with both the electrolyte and CO_2. With a hydrophilic binder, these boundaries are located only at the electrolyte–MPL interface, because the surface of the catalyst is covered by the electrolyte (Figure 7c). When a hydrophobic binder such as FEP is used, the catalyst is only partially in contact with the electrolyte due to the water-repellent properties of the binder. A microhydrophobic environment is created around the FEP molecules and allows CO_2 to access surfaces of the catalyst that are located far away from the electrolyte–MPL interface, thus enhancing CO_2RR (Figure 7d). Furthermore, in both configurations, a high concentration of CO_2 near FEP can

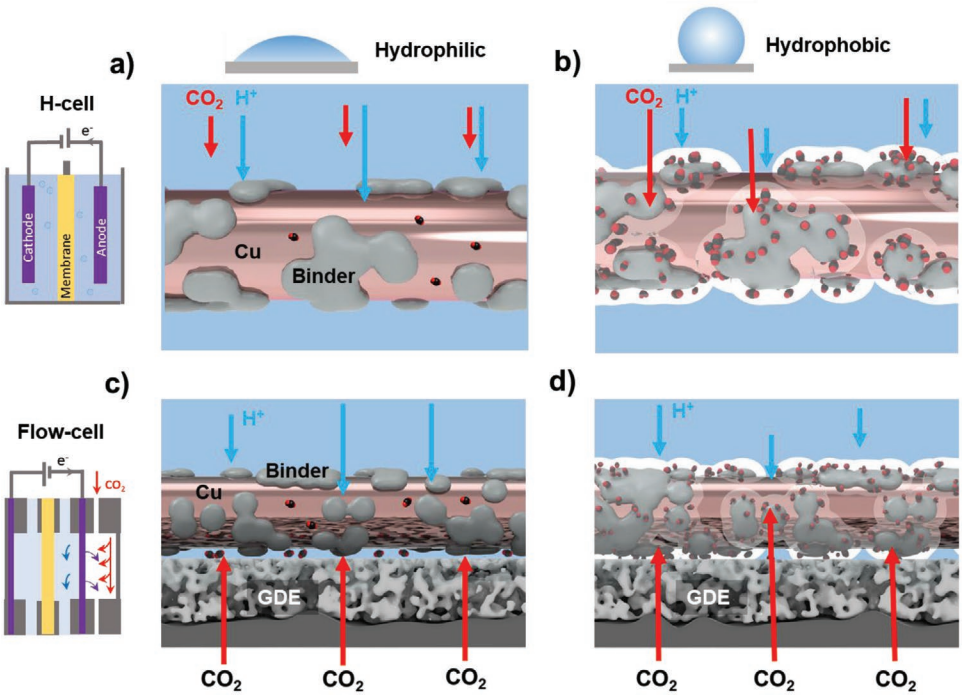

Figure 7. Schematic illustration of the local reaction environment near the Cu surface with a,c) hydrophilic and b,d) hydrophobic polymer binders in an H-cell (a, b) and flow cell (c, d). Electrolyte (light blue), Cu (brownish red), polymer binder (gray), trapped CO_2 in hydrophobic samples (white), CO_2 pathway (red arrow), and H^+ pathway (blue arrow).

result in a high production rate of CO; this, combined with the enhanced accessibility of CO to the catalyst surface, improves the selectivity of C_{2+}.

3. Conclusions

In summary, we show that coating the surface of Cu catalysts with a thin layer of polymer binder is a simple but effective method for tuning the CO_2RR activity and selectivity. This is because polymer binders not only bond catalyst powders on the support but also change the local concentration of reactants (i.e., CO_2 and H_2O) near the catalyst surface, thus altering the CO_2RR performance. Specifically, a hydrophobic polymer binder (i.e., FEP) can facilitate the access of CO_2 to the Cu surface, thereby promoting the production and accumulation of the key reaction intermediate CO, and resulting in an increase in the production of C_{2+} products. Our results show that a Cu catalyst coated with an FEP binder achieved ≈52% faradaic efficiency toward C_{2+} products in an H-cell. In a flow reactor, a partial current density of more than 600 mA cm^{-2} was obtained for C_{2+} products with ≈77% faradaic efficiency. Therefore, our findings highlight that, in addition to modifying the intrinsic properties of the catalyst, controlling the local concentration of the reactants by tuning the hydrophobicity of the catalyst with a proper polymer binder can also greatly improve the performance of CO_2RR.

4. Experimental Section

Synthesis of the CuO Catalyst: The CuO catalyst was synthesized using a precipitation method adapted from a previous publication.[49] $Cu(NO_3)_2{\cdot}3H_2O$ (1.3 g; Sigma-Aldrich) was dissolved in 100 ml of Milli-Q water, followed by the addition of 30 ml of 0.15 M NH_4OH prepared from ammonium hydroxide, 28% NH_3 (Alfa Aesar). Following this, 10 ml of 1.0 M NaOH (Reactolab SA) was introduced at a rate of 2 ml min^{-1}. The precipitation reaction was carried out for 30 min while being continuously stirred with a magnetic agitator. The obtained $Cu(OH)_2$ precipitate was then washed thoroughly with deionized water and ethanol in a centrifuge. Finally, the $Cu(OH)_2$ precipitate was freeze-dried for 72 h and calcined in air for 1 h at 300 °C to obtain the CuO catalyst.

Working Electrode Preparation: The catalyst ink was prepared by dispersing the as-synthesized CuO catalyst in isopropanol (IPA, ≥99.8%, analytical reagent grade, Fisher Scientific). Polyacrylic acid (PAA, 63 wt.% solution in water, Fisher Scientific), Nafion (5 wt.% in a mixture of lower aliphatic alcohols and water, Sigma-Aldrich), and fluorinated ethylene propylene (FEP, 50 wt.% dispersion in water, FuelCellStore) were used as binders across three separate samples. The chemical formulae of the three polymers are shown in Figure S3 (Supporting Information). The dispersion (containing 0.2 mg of polymer binder and 0.25 ml of solvent for every mg of catalyst) was sonicated for 10 min, then drop-casted onto the carbon paper (H-cell: Toray Carbon Paper, TGP-H-60, Alfa Aesar; Flow cell: YLS-30T, Suzhou Sinero Technology Co.) with a loading of 0.4 mg cm^{-2}. The obtained working electrodes were denoted as Cu-PAA, Cu-Nafion, and Cu-FEP, respectively.

Performance Test: A potentiostat (Metrohm Autolab PGSTAT302N) was used to perform electrochemical measurements. The gas products were quantified using an online gas chromatograph (GC, SRI instruments 8610C), which was equipped with a thermal conductivity detector (TCD) and a flame ionization detector (FID). A series of standard gases with different concentrations of CO, CH_4, C_2H_4, and C_2H_6 were used to calibrate the GC (Equation S1). The electrolyte was collected after the chronoamperometric measurement, and ^1H nuclear magnetic resonance (NMR) was used to quantify liquid products (Bruker 400 MHz AVIII HD). A mixture of methanol, ethanol, *n*-propanol, acetic acid, acetone, and formic acid with a predefined concentration was used to construct a calibration curve. The concentrations of the liquid mixtures used for calibration ranged from 0.067 to 10 mM (Equation S2, Figure S6, and Table S1 Supporting Information).

The electrochemical cell was an H-shaped, gas-tight cell composed of two compartments: one for the oxygen evolution reaction (OER), and one for the CO_2RR. An ion-exchange membrane (Nafion 212, Dupont) was used to separate the two compartments. The cathode compartment was composed of an Ag/AgCl reference electrode and a working electrode with the catalyst of interest. CO_2 was continuously bubbled into the 0.1 M $KHCO_3$ catholyte both before and during the CO_2RR. A Pt wire was used as a counter electrode in the anode compartment. The electrochemical measurements in the flow reactor were performed using a previously reported system.[17] The CO_2 flow rate was kept at 110 ml min^{-1}. The constant potential mode was used for H-cell measurements and the constant current mode was used for flow-cell measurements. All potentials were reported after iR correction.

Materials Characterization: Scanning electron microscopy (SEM) images were acquired on a Thermofisher Teneo FE-SEM, and high-resolution transmission electron microscopy (HR-TEM) images were obtained with a Thermofisher Tecnai Osiris 200kV TEM. The energy-filtered TEM (EF-TEM) images were acquired using a JEOL 2200FS TEM. EFTEM carbon elemental maps were performed using the three window-method on the carbon K edge in electron energy-loss spectra (EELS). The X-ray diffraction (XRD) spectra were acquired using a Bruker D8 Advance system using Cu Kα ($\lambda = 1.54$ Å) radiation. X-ray photoelectron spectroscopy (XPS) was performed with a Kratos Axis Supra XPS system, using a monochromated Al Ka (1486.61 eV) X-ray source at a nominal power of 225 W. A pass energy of 20 eV was used for acquiring the C 1s, O 1s, and Cu 2p core-level spectra. The Water Contact Angle (WCA) and the Captive Bubble Contact Angle (CBCA) were measured with a Kruss EasyDrop Drop Shape Analyzer.

Operando Raman Measurements: Surface-enhanced operando Raman spectroscopy was performed using a home-built Raman cell. The incident and scattered beams were sent to the sample and collected through an immersion objective, respectively (Leica, 63×). A red light with a wavelength of 632 nm was used as the laser beam. $KHCO_3$ (0.1 M) was used as the electrolyte and CO_2 was purged continuously to the cathodic compartment both before and during the Raman measurements.

Supporting Information

Supporting Information is available from the Wiley Online Library or from the author.

Acknowledgements

This research was supported by Swiss National Science Foundation (Ambizione Project No. PZ00P2_179989). This research was also part of the activities of SCCER HeE, which was financially supported by Innosuisse-Swiss Innovation Agency.

Open access funding provided by Ecole Polytechnique Federale de Lausanne.

Conflict of Interest

The authors declare no conflict of interest.

Data Availability Statement

The data that support the findings of this study are available from the corresponding author upon reasonable request.

Keywords

CO_2 reduction, copper catalysts, electrocatalysis, hydrophobicity, polymer binders

Received: November 22, 2021
Published online: January 5, 2022

[1] N. S. Lewis, D. G. Nocera, *Proc. Natl. Acad. Sci. USA* **2006**, *103*, 15729.
[2] T. R. Cook, D. K. Dogutan, S. Y. Reece, Y. Surendranath, T. S. Teets, D. G. Nocera, *Chem. Rev.* **2010**, *110*, 6474.
[3] P. De Luna, C. Hahn, D. Higgins, S. A. Jaffer, T. F. Jaramillo, E. H. Sargent, *Science* **2019**, *364*, eaav3506.
[4] H. B. Gray, *Nat. Chem.* **2009**, *1*, 7.
[5] L. Schlapbach, A. Züttel, *Nature* **2001**, *414*, 353.
[6] R. Reske, H. Mistry, F. Behafarid, B. Roldan Cuenya, P. Strasser, *J. Am. Chem. Soc.* **2014**, *136*, 6978.
[7] F. S. Roberts, K. P. Kuhl, A. Nilsson, *Angew. Chemie Int Ed.* **2015**, *54*, 5179.
[8] A. Loiudice, P. Lobaccaro, E. A. Kamali, T. Thao, B. H. Huang, J. W. Ager, R. Buonsanti, *Angew. Chemie Int Ed.* **2016**, *55*, 5789.
[9] W. Luo, J. Zhang, M. Li, A. Züttel, *ACS Catal.* **2019**, *9*, 3783.
[10] W. Luo, W. Xie, M. Li, J. Zhang, A. Züttel, *J. Mater. Chem. A* **2019**, *7*, 4505.
[11] X. Feng, K. Jiang, S. Fan, M. W. Kanan, *ACS Cent. Sci.* **2016**, *2*, 169.
[12] C. G. Morales-Guio, E. R. Cave, S. A. Nitopi, J. T. Feaster, L. Wang, K. P. Kuhl, A. Jackson, N. C. Johnson, D. N. Abram, T. Hatsukade, C. Hahn, T. F. Jaramillo, *Nat. Catal.* **2018**, *1*, 764.
[13] D. Ren, B. S. H. Ang, B. S. Yeo, *ACS Catal.* **2016**, *6*, 8239.
[14] J. Gao, H. Zhang, X. Guo, J. Luo, S. M. Zakeeruddin, D. Ren, M. Grätzel, *J. Am. Chem. Soc.* **2019**, *141*, 18704.
[15] W. Luo, W. Xie, R. Mutschler, E. Oveisi, G. L. De Gregorio, R. Buonsanti, A. Züttel, *ACS Catal.* **2018**, *8*, 6571.
[16] L.-C. Weng, A. T. Bell, A. Z. Weber, *Phys. Chem. Chem. Phys.* **2018**, *20*, 16973.
[17] J. Zhang, W. Luo, A. Züttel, *J. Catal.* **2020**, *385*, 140.
[18] J. Zhang, W. Luo, A. Züttel, *J. Mater. Chem. A* **2019**, *7*, 26285.
[19] K. Yang, R. Kas, W. A. Smith, T. Burdyny, *ACS Energy Lett.* **2021**, *6*, 33.
[20] N. T. Nesbitt, T. Burdyny, H. Simonson, D. Salvatore, D. Bohra, R. Kas, W. A. Smith, *ACS Catal.* **2020**, *10*, 14093.
[21] D. Wakerley, S. Lamaison, F. Ozanam, N. Menguy, D. Mercier, P. Marcus, M. Fontecave, V. Mougel, *Nat. Mater.* **2019**, *18*, 1222.
[22] Z. Cai, Y. Zhang, Y. Zhao, Y. Wu, W. Xu, X. Wen, Y. Zhong, Y. Zhang, W. Liu, H. Wang, Y. Kuang, X. Sun, *Nano Res. 2018 122* **2018**, *12*, 345.
[23] F. P. García de Arquer, C. T. Dinh, A. Ozden, J. Wicks, C. McCallum, A. R. Kirmani, D. H. Nam, C. Gabardo, A. Seifitokaldani, X. Wang, Y. C. Li, F. Li, J. Edwards, L. J. Richter, S. J. Thorpe, D. Sinton, E. H. Sargent, *Science* **2020**, *367*, 661.
[24] Y. C. Tan, K. B. Lee, H. Song, J. Oh, *Joule* **2020**, *4*, 1104.
[25] G. H. Simon, C. S. Kley, B. R. Cuenya, *Angew. Chem., Int. Ed.* **2021**, *60*, 2561.
[26] D. Ren, Y. Deng, D. Handoko, C. S. Chen, S. Malkhandi, B. S. Yeo, *ACS Catal.* **2015**, *5*, 2814.
[27] S. Khan, J. Hwang, Y. S. Horn, K. K. Varanasi, *Cell Reports Phys. Sci.* **2021**, *2*, 100318.
[28] M. Ma, K. Djanashvili, W. A. Smith, *Angew. Chem., Int. Ed.* **2016**, *55*, 6680.
[29] M. Wang, L. Wan, J. Luo, *Nanoscale* **2021**, *13*, 3588.
[30] A. Herzog, A. Bergmann, H. S. Jeon, J. Timoshenko, S. Kühl, C. Rettenmaier, M. Lopez Luna, F. T. Haase, B. Roldan Cuenya, *Angew. Chem., Int. Ed.* **2021**, *60*, 7426.
[31] Y. Lum, J. W. Ager, *Angew. Chem., Int. Ed.* **2018**, *57*, 551.
[32] A. Dutta, I. Z. Montiel, R. Erni, K. Kiran, M. Rahaman, J. Drnec, P. Broekmann, *Nano Energy* **2020**, *68*, 104331.
[33] F. Scholten, K. L. C. Nguyen, J. P. Bruce, M. Heyde, B. R. Cuenya, *Angew. Chem., Int. Ed.* **2021**, *60*, 19169.
[34] C. Kim, J. C. Bui, X. Luo, J. K. Cooper, A. Kusoglu, A. Z. Weber, A. T. Bell, *Nat. Energy* **2021**, *6*, 1026.
[35] D. Ren, J. Gao, L. Pan, Z. Wang, J. Luo, S. M. Zakeeruddin, A. Hagfeldt, M. Grätzel, *Angew. Chemie* **2019**, *131*, 15178.
[36] H. Jung, S. Y. Lee, C. W. Lee, M. K. Cho, D. H. Won, C. Kim, H. S. Oh, B. K. Min, Y. J. Hwang, *J. Am. Chem. Soc.* **2019**, *141*, 4624.
[37] T. Möller, F. Scholten, T. N. Thanh, I. Sinev, J. Timoshenko, X. Wang, Z. Jovanov, M. Gliech, B. Roldan Cuenya, A. S. Varela, P. Strasser, *Angew. Chemie* **2020**, *132*, 18130.
[38] Z.-Z. Niu, F.-Y. Gao, X.-L. Zhang, P.-P. Yang, R. Liu, L.-P. Chi, Z.-Z. Wu, S. Qin, X. Yu, M.-R. Gao, *J. Am. Chem. Soc.* **2021**, *143*, 8011.
[39] S. Ma, M. Sadakiyo, R. Luo, M. Heima, M. Yamauchi, P. J. A. Kenis, *J. Power Sources* **2016**, *301*, 219.
[40] C. Reller, R. Krause, E. Volkova, B. Schmid, S. Neubauer, A. Rucki, M. Schuster, G. Schmid, *Adv. Energy Mater.* **2017**, *7*, 1602114.
[41] K. K. Patra, S. Park, H. Song, B. Kim, W. Kim, J. Oh, *ACS Appl. Energy Mater.* **2020**, *3*, 11343.
[42] P. O. Larsson, A. Andersson, *J. Catal.* **1998**, *179*, 72.
[43] L. Debbichi, M. C. Marco De Lucas, J. F. Pierson, P. Krü, **2012**, *116*, 10232.
[44] S. Jiang, K. Klingan, C. Pasquini, H. Dau, *J. Chem. Phys* **2019**, *150*, 041718.
[45] X. Chang, Y. Zhao, B. Xu, *ACS Catal.* **2020**, *10*, 13737.
[46] C. Zhan, F. Dattila, C. Rettenmaier, A. Bergmann, S. Kühl, R. García-Muelas, N. López, B. R. Cuenya, *ACS Catal.* **2021**, 7694.
[47] P. Zhang, J. Cai, Y. X. Chen, Z. Q. Tang, D. Chen, J. Yang, D. Y. Wu, B. Ren, Z. Q. Tian, *J. Phys. Chem. C* **2010**, *114*, 403.
[48] M. Moradzaman, G. Mul, *ChemElectroChem* **2021**, *8*, 1478.
[49] J. J. Lv, M. Jouny, W. Luc, W. Zhu, J. J. Zhu, F. Jiao, *Adv. Mater.* **2018**, *30*, 1803111.